Conference Paper, Published Version

Park, Seong Soo; Kim, Hyung-Jun; Yoo, Jeseon; Cho, Yong-Sik

Simulation of Flood Propagation Due to Levee Break Using the Cartesian Cut Cell Method

SIMULATION OF FLOOD PROPAGATION DUE TO DAM-BREAK USING THE CARTESIAN CUT-CELL METHOD

Seongsoo Park[1], Hyung-Jun Kim[2], Jeseon Yoo[3] and Yong-Sik Cho[4]

[1] Graduate Student, Department of Civil Engineering, Hanyang University
17 Haengdang-dong, Seongdong-gu, Seoul 133-791, Korea, e-mail: reibun@hanyang.ac.kr
[2] Graduate Student, Department of Civil Engineering, Hanyang University
17 Haengdang-dong, Seongdong-gu, Seoul 133-791, Korea, e-mail: john0705@hanyang.ac.kr
[3] Post-doctoral Researcher, Department of Civil Engineering, Hanyang University
17 Haengdang-dong, Seongdong-gu, Seoul 133-791, Korea, e-mail: jeseonyoo@hanyang.ac.kr
[4] Corresponding Author, Department of Civil Engineering, Hanyang University
17 Haengdang-dong, Seongdong-gu, Seoul 133-791, Korea, e-mail: ysc59@hanyang.ac.kr

ABSTRACT

The precise representation of the complex geometry still remains the challengeable problems in the computational hydraulics. In this study, we develop a numerical model based on a finite volume approach with the Cartesian cut-cell mesh. The HLLC approximate Riemann solver is employed to discretize the advective terms in the governing equations. TVD-WAF method is applied to management of oscillations near discontinuities with a second-order accurancy. To verify the model, steady flow convergence over an irregular bathymetry is carried out. Two types of upstream and downstream boundary conditions induce two cases of transient flows. These numerical results are compared with analytical solutions. Finally, flood wave propagation through 45° bended channel is simulated and compared with experimental measurements. The model consistently presents accurate and reliable results for all cases.

Keyword: Cartesian cut-cell grids, shallow-water equations, flood inundation, levee break

1. INTRODUCTION

Dam-break flows constitute an important problem in water resource engineering. The interest of studying this phenomenon resides not only its practical importance for modeling but also a fundamental interest in fluid mechanics. There are many numerical methods for dam-break flows with finite-difference or finite-volume method. Bermudez and Va´zquez (1994) proposed an upwind method in the shallow water equations and LeVeque (1998) developed a treatment for the bed slope source terms which balanced source terms and flux gradients. The method can provide an accurate solution for a quasi-steady problem, but it is difficult to apply to steady transcritical flow with shock waves. Hubbard and Garcia-Navarro (2000) proposed a scheme that balanced source terms and flux gradients. Jian *et al* (2004) simulated dam-break flows in general geometries with the cut-cell mesh using HLLC and surface gradient method. In this study, the finite volume method is applied to discretize the hyperbolic conservative forms of shallow-water equations. Approximate Riemann solver is applied to calculate the advective fluxes in the governing equations. TVD-WAF method is applied to management of numerical discontinuities with second-order accuracy in space and time.

The Cartesian cut-cell method easily represents complex domain considering boundary geometry by cutting the uniform Cartesian mesh compared with the traditional mesh generation such as boundary-fitted curvilinear coordinate or unstructured grids with irregularly shaped mesh. To generate the Cartesian cut-cell mesh, it needs essential information about boundaries and shifting of segment positions. The accuracy of generated cut-cell mesh is affected by how to shift segment positions to compensate the cutted grids. In former research of Ingram *et al*. (2003), the segments are shifted to left-lower corner of mesh by integer point assumptions. However, this regardless assumption of segment shifting produces apparent geometrical errors. Therefore, the cut-cell generation technique is improved by a new shifting method for start and exit segment positions in this study.

2. CUT-CELL METHOD

A Cartesian cut-cell mesh is generated by "cutting" solid bodies out of a background Cartesian mesh. The results of cutting cells are classified into fluid, solid and cut grid cells as shown in Fig. 1. In order to generate the cut-cells, the body surfaces are represented using polylines, whose knots are defined in an anti-clockwise direction as follows;

$$P_i = \{(x_0, y_0), \cdots, (x_j, y_j), \cdots (x_n, y_n)\} \tag{1}$$

To find intersection points of a particular line segment, defined by its start and end coordinates (x_s, y_s) and (x_e, y_e), are found as follows. Ingram *et al*. (2003) suggested the address (I_s, J_s) of the cell containing the start coordinate is computed.

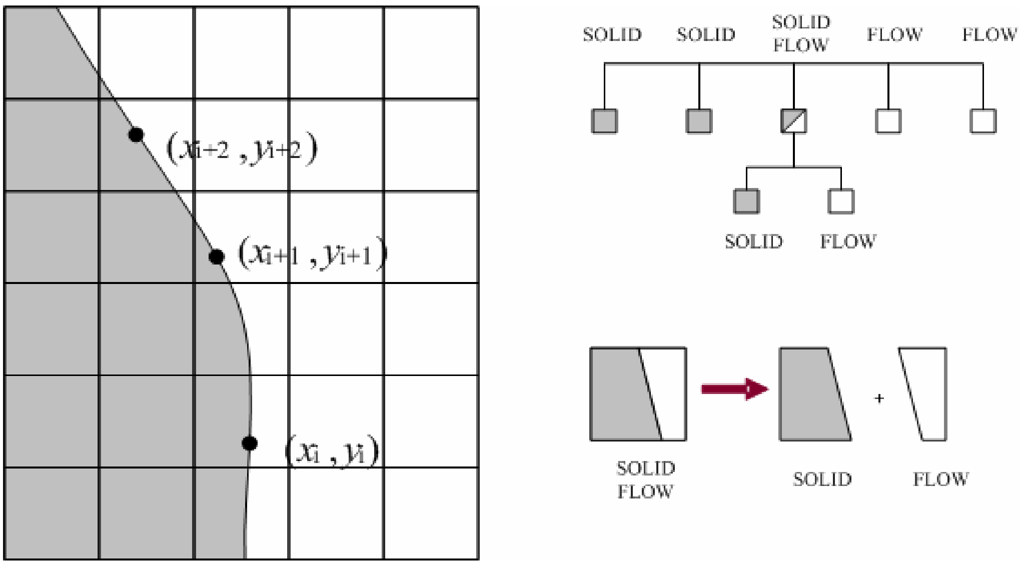

Figure 1 Segment points and cut-cells of irregular geometry

$$I_s = \text{int}\left(\frac{x_s - x_0}{\Delta x}\right), \quad J_s = \text{int}\left(\frac{y_s - y_0}{\Delta y}\right) \tag{2}$$

where x_0 and y_0 are the coordinates of the bottom left corner of the computational domain. The address (I_e, J_e) of the end point is similarly found. For convenience, the next points of cutting mesh can be found with the calculated line slope along the line. The slope of the line can be calculated as

$$S_{line} = \frac{y_e - y_s}{x_e - x_s} \tag{3}$$

the second point (x_2, y_2) from the start point (x_s, y_s) can be assumed to be two situations like Eqs.1 and 2. ΔL_a is the distance between start point and (x_2^a, y_2^a), ΔL_b is the distance between start point and (x_2^b, y_2^b). The next closest point is the nearst cutting point. Similar to find the second cutting point, all position of cutting points can be calculated upto the exit point, (x_e, y_e).

In this work, an improved method is proposed concerning the accuracy of the position of start and exit points. In the study of Ingram *et al*. (2003), start and exit segments are shifted only to an edge node for simple numerical treatments. This assumption may affect the accuracy of geometry representation with large base grids. Thus, an assumption about shifting the segment plays an important role in accurate cut-cell generation. In this study, for more accurate cut-cell grids of the segments are displaced to the nearest point on mesh edge. The new assumption of finding the start and exit segment point is also very simple. With a position of segment point (x_i, y_i) and base grid size, four distances can be ascertained from a segment point to mesh edge like in Fig. 2 and Eq. 4

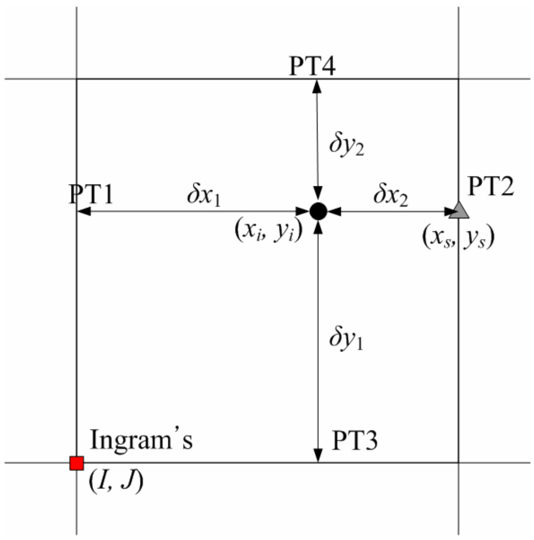

Figure 2 An improved method for shifting start and exit points

$$\begin{aligned} \delta x_1 &= \mathrm{MOD}(x_s, \Delta x) \qquad & \delta x_2 &= \Delta x - \mathrm{MOD}(x_s, \Delta x) = \Delta x - \delta x_1 \\ \delta y_1 &= \mathrm{MOD}(y_s, \Delta y) \qquad & \delta y_2 &= \Delta y - \mathrm{MOD}(y_s, \Delta y) = \Delta y - \delta y_1 \end{aligned} \tag{4}$$

where δx_1 is the x-directional distance from the west side and δy_1 is the y-directional distance from south side of mesh edge to segment point. These can be calculated by MOD function with segment point (x_i, y_i) and spatially mesh size $(\Delta x, \Delta y)$. δx_2 and δy_2 are remaining distance easily calculated by δx_1 and δy_1.

By computing four distances, possibly, four shifted points are concerned as PT1, PT2, PT3 and PT4 as depicted in Fig. 2. In order to minimize the error due to the distorted position, the closest point is selected as Eq. 5.

$$\begin{aligned}
(x_s, y_s) &= (x_i - \delta x_1 \ , \ y_i) && \text{if} \quad \delta x_1 = \min(\delta x_1, \delta x_2, \delta y_1, \delta y_2) \\
(x_s, y_s) &= (x_i + \delta x_2 \ , \ y_i) && \text{if} \quad \delta x_2 = \min(\delta x_1, \delta x_2, \delta y_1, \delta y_2) \\
(x_s, y_s) &= (x_i \ , \ y_i - \delta y_1) && \text{if} \quad \delta y_1 = \min(\delta x_1, \delta x_2, \delta y_1, \delta y_2) \\
(x_s, y_s) &= (x_i \ , \ y_i + \delta y_2) && \text{if} \quad \delta y_2 = \min(\delta x_1, \delta x_2, \delta y_1, \delta y_2)
\end{aligned} \tag{5}$$

3. NUMERICAL SCHEME

Governing equations

The two-dimensional shallow-water equations in conservative form are given as

$$\frac{\partial \mathbf{U}}{\partial t} + \frac{\partial \mathbf{E}}{\partial x} + \frac{\partial \mathbf{F}}{\partial y} = \mathbf{S} \tag{6}$$

in Eq. 6, the vector of conserved variables $\mathbf{U}$, the flux vectors $\mathbf{E}$ and $\mathbf{F}$ in x and y directions, and the source term $\mathbf{S}$ can be written as

$$\mathbf{U} = \begin{bmatrix} d \\ du \\ dv \end{bmatrix}, \quad \mathbf{E} = \begin{bmatrix} du \\ du^2 + \frac{1}{2} g d^2 \\ duv \end{bmatrix}, \quad \mathbf{F} = \begin{bmatrix} dv \\ duv \\ dv^2 + \frac{1}{2} g d^2 \end{bmatrix}, \quad \mathbf{S} = \begin{bmatrix} 0 \\ gd(S_{ox} - S_{fx}) \\ gd(S_{oy} - S_{fy}) \end{bmatrix} \tag{7}$$

where d = total water depth, u and v = velocity components in the x and y directions, g = acceleration due to gravity, and S_{ox} and S_{oy} = bed slope components in the x and y directions, respectively. The bottom frictions S_{fx} and S_{fy} have been estimated by using the Manning's empirical formula expressed as

$$S_{fx} = \frac{un^2\sqrt{u^2+v^2}}{d^{4/3}}, \quad S_{fy} = \frac{vn^2\sqrt{u^2+v^2}}{d^{4/3}} \tag{8}$$

in which n = Manning's roughness coefficient.

Finite volume method on an unstructured grid system

The finite volume method (FVM) is an approach for dealing with a general unstructured grid. The major advantages of FVM are: an ability to use a flexible grid system, such as triangles or quadrilaterals suitable for more complex geometries, use of an integral conservation law, and a close relationship between a fractional step method and FVM.

By integrating Eq. 6 over an arbitrary cell, the basis equation of the FVM can be obtained as

$$\frac{\partial}{\partial t}\int_A \mathbf{U}dA + \oint_\Omega \mathbf{G}\cdot n d\Omega = \oint_\Omega \mathbf{S}d\Omega \tag{9}$$

where $\mathbf{G}$ = flux tensor; A and Ω = surface area and boundary of the control volume L, respectively and n =outward unit vector normal to the boundary. By assuming the x-direction as the reference direction and using the rotational invariance, the flux becomes

$$\mathbf{G}\cdot n = \mathbf{T}_s^{-1}\mathbf{G}\left(\mathbf{T}_s\mathbf{U}\right) \tag{10}$$

by substuting Eq. 9, Eq. 10 becomes Eq.11.

$$\frac{d\mathbf{U}}{dt} + \frac{1}{|A|}\sum_{s=1}^{N}\int_{A_s}^{A_{s+1}} \mathbf{T}_s^{-1}\mathbf{G}\left(\mathbf{T}_s\mathbf{U}\right)dA = \mathbf{S} \tag{11}$$

into Eq.4, the integrations become as Eg.11.

HLLC approximate Riemann solver

Harten *et al.* (1983) presented a scheme for solving the Riemann problem approximately. The scheme, known as HLL approximate Riemann solver, assumes a wave configuration for the solution that consists of two waves separating three constants. An advantage of the HLL approximate Riemann solver is that it uses wave speeds based on analytic dry front speeds, consequently, it produces better results than Roe's solver on a dry bed.

In governing Eq. 6, $\mathbf{U}$ is a vector of three conserved variables. In solving the flux part, the solution to the Riemann problem consists of three waves with speeds $\mathbf{S}$ separating four constant states. Therefore, for two-dimensional shallow-water equations, the assumption of the HLL scheme that two waves separated by three constants is incorrect. To overcome the shortcoming of the HLL scheme, a modification called the HLLC approximate Riemann solver was suggested by Fraccarollo and Toro (1995). This is correct for two-dimensional shallow-water equation.

The HLLC approximated Riemann solver is given as

$$\tilde{\mathbf{U}}(x,y) = \begin{cases} \mathbf{U}_L & for \quad 0 \le S_L \\ \mathbf{U}_L^* & for \quad S_L \le 0 \le S_* \\ \mathbf{U}_R^* & for \quad S_* \le 0 \le S_R \\ \mathbf{U}_R & for \quad S_R \le 0 \end{cases} \tag{12}$$

in order to determine numerical fluxes in the HLLC Riemann solver, wave speeds in Eq. 12 should be estimated. The estimated wave speeds, in this study, are given as

$$\begin{aligned} S_L &= \min\left(u_L - \sqrt{gd_L}\,,\, u_* - \sqrt{gd_*}\right) \\ S_* = u_* &= \frac{u_L + u_R}{2} + \sqrt{gd_L} - \sqrt{gd_R} \\ S_R &= \max\left(u_R + \sqrt{gd_R}\,,\; u_* + \sqrt{gd_*}\right) \end{aligned} \tag{13}$$

in the view of Eq. 12, the HLLC flux can be written as

$$\mathbf{E}_{i=1/2}^{HLLC} = \begin{cases} \mathbf{E}_L & for \quad 0 \le S_L \\ \mathbf{E}_L^* = E_L + S_L\left(\mathbf{U}_L^* - \mathbf{U}_L\right) & for \quad S_L \le 0 \le S_* \\ \mathbf{E}_R^* = E_R + S_R\left(\mathbf{U}_R - \mathbf{U}_R^*\right) & for \quad S_* \le 0 \le S_R \\ \mathbf{E}_R & for \quad S_R \le 0 \end{cases} \tag{14}$$

where the subscript $i+1/2$ means an intercell boundary between L and R. More details of the HLLC approximate Riemann solver are described in Toro (1999) and Billett and Toro (1997).

TVD-WAF scheme

The second-order accurate WAF scheme is given as

$$\mathbf{E}_{i+1/2} = \frac{1}{2}\left(\mathbf{E}_i + \mathbf{E}_{i+1}\right) - \frac{1}{2}\sum_{k=1}^{N} c_k \Delta\mathbf{E}_{i+1/2}^k \tag{15}$$

where $\mathbf{E}_{i+1/2}^k = \mathbf{E}\left(\mathbf{U}_{i+1/2}^k\right)$ can be replaced by Eq. 14, c_k = Courant number for a wave k of speed S_k, and $\Delta\mathbf{E}_{i+1/2}^k$ is given as

$$\Delta\mathbf{E}_{i+1/2}^k = \mathbf{E}_{i+1/2}^{k+1} - \mathbf{E}_{i+1/2}^k \tag{16}$$

in order to control a non-physical oscillation commonly observed in a second-order accurate scheme, the TVD scheme is employed. The TVD version of the WAF scheme is given as

$$\mathbf{E}_{i+1/2} = \frac{1}{2}\left(\mathbf{E}_i + \mathbf{E}_{i+1}\right) - \frac{1}{2}\sum_{k=1}^{N} sign\left(c_k\right)\varphi_{i+1/2}^k \Delta\mathbf{E}_{i+1/2}^k \tag{17}$$

where $\varphi_{i+1/2}^k$ = WAF limiter function and is given as

$$\varphi(r,k)=\begin{cases}1 & for \quad r\le 0\\ 1-2\left(1-|c_k|\right)r & for \quad 0\le r\le 1/2\\ |c_k| & for \quad 1/2\le r\le 1\\ 1-\left(1-|c_k|\right)r & for \quad 1\le r\le 2\\ 2|c_k|-1 & for \quad 2\le r\end{cases} \tag{18}$$

where r = ratio of the upwind change to a local change and is given as

$$r_{i+1/2}=\frac{\Delta upwind}{\Delta local}=\begin{cases}\dfrac{\Delta u_{i-1/2}^k}{\Delta u_{i+1/2}^k} & for \quad c_k>0\\ \dfrac{\Delta u_{i+3/2}^k}{\Delta u_{i+1/2}^k} & for \quad c_k<0\end{cases} \tag{19}$$

where $\Delta u_{i+1/2}^k$ is given as $u_{i+1}^k-u_i^k$.

4. NUMERICAL TESTS AND RESULTS

Steady flow over a hump

In this study, two cases of flow over a hump are tested to study the conservation and convergence of the numerical model to steady states over irregular bathymetry. This is a classical test problem considered by various authors (Goutal and Maurel, 1997; Văsquez-Cendón, 1999; Zhou *et al*., 2001; Gallouët, 2003). The breath of channel is constantly $b(x,h)=1.0m$ and the length is $L=25.0m$. The channel bottom has a hump which elevation is defined as Eq. 21. In these cases bottom friction is neglected.

$$\begin{aligned} z_b(x)&=0.2-0.05(x-10)^2 && \text{if} \quad 8<x<12\\ &=0 && \text{else}\end{aligned} \tag{20}$$

According to the boundary conditions at upstream and downstream, the flow will be converged as subcritical, supercritical or transcritical with a hydraulic jump. Goutal (1997) derived exact solutions to compare and validate the numerical accuracies using the Bernoulli theorem and the principle of momentum conservation.

The tolerance for the convergence state is $\varepsilon=10^{-5}$, and the spatial grid size is set as $\Delta x=0.1m$. The first case of numerical test is the simulation of subcritical flow. The upstream boundary condition imposes the discharge $Q=4.42m^3/\sec$, whereas water depth of downstream is set as $h_{down}=2.0m$. In Figs. 3, the simulated results of water level is compared with exact solutions. This is a good agreement with numerical results and analytic solutions.

The next problem of numerical test is a transcritical flow without hydraulic jump. At the upstream boundary, discharge is set as $Q=1.53m^3/\sec$ and downstream water depth and velocity are given by transmissive boundary conditions. As seen in Figs. 4, the flow converges on the supercritical flow at downstream end. The resulting downstream depth is

$h_{down} = 2.0m$ and velocity is $u_{down} = 2.0m$. The present model shows good result compared to exact solutions about water surface level.

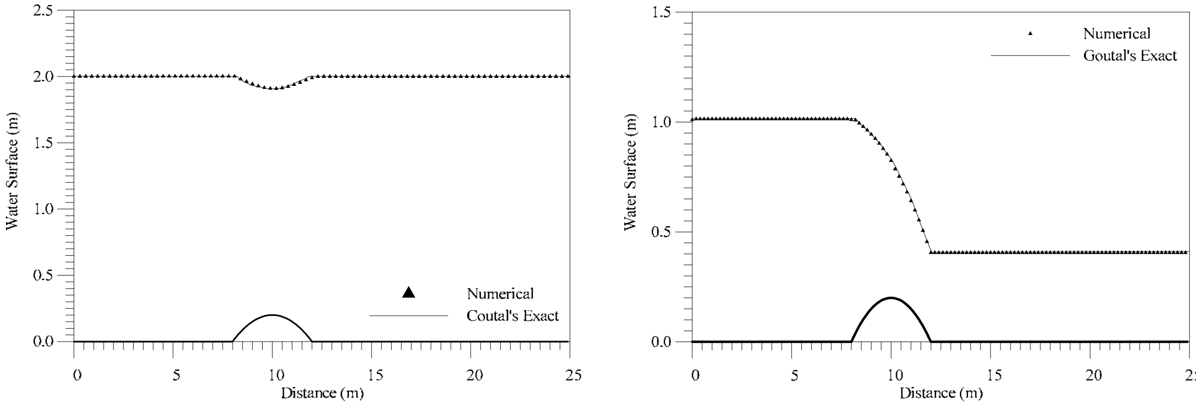

(a) Subcritical flow over a hump   (b) Transcritical flow over a hump

Figure 3 Comparisons of free surface with exact solutions

Dam-break flow through 45° bend channel

The second test case is dam-break propagation through the experiment channel contains a 45° bend as shown in Fig. 5. This experiment has been involved in the CADAM project (Morris, 2000). The bed of the reservoir is once again 0.33 m below that of the channel, forming a vertical step at the entrance to the channel. The initial water depth in the reservoir was 0.58 m.

A base Cartesian mesh, with spatial grid size $\Delta x = \Delta y = 0.05m$, was used to discretize the flow domain and the Cartesian cut-cell method used to align the mesh with both the solid walls.

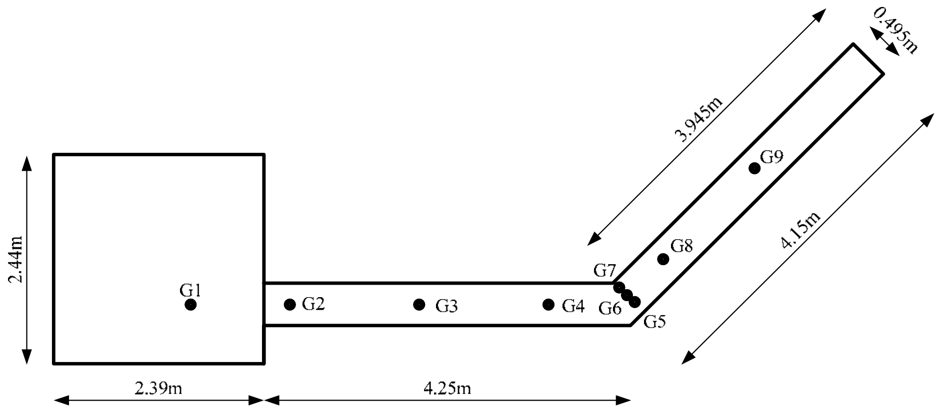

Figure 4 Plan view of a channel with a 45° bend

Fig. 5 shows comparisons of water depth with measured data (Morris, 2000) and numerical results of present model at gauge points G3, G5 and G9. The results of the present model agree with the experimentally measured data.

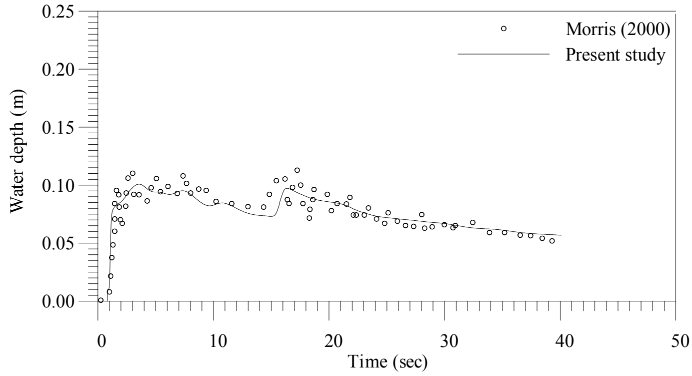

(a) At gauge point G3

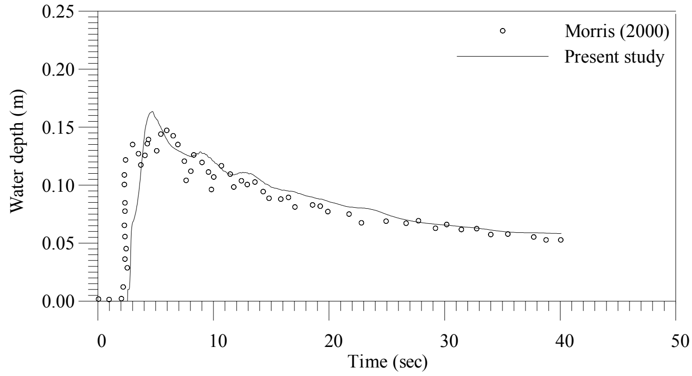

(b) At gauge point G5

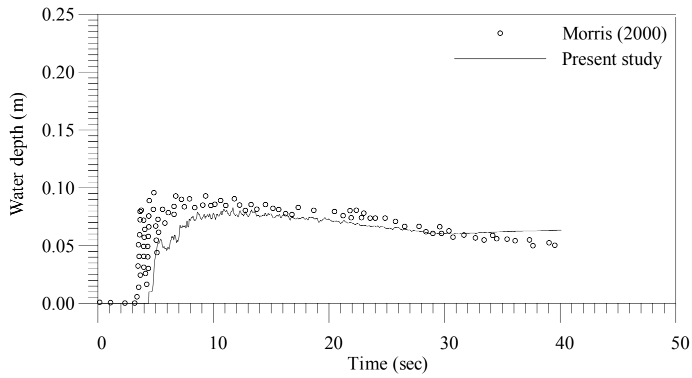

(c) At gauge point G9

Figure 5 Comparisons of water depth variation with Morris (2000)

5. CONCLUSION

In this study, a finite volume numerical model with the Cartesian cut-cell method is employed to two-dimensional shallow-water equations. In order to discretize the governing equations, HLLC approximate Riemann solver and TVD-WAF method are applied to calculation of the numerical fluxes.

Numerical accuracies of approximate Riemann solver have been tested by simulations of steady flow over irregular bathymetry. In one-dimensional tests, numerical results have been compared with solutions which are derived from Bernoulli theorem, momentum conservation law for transcritical flow. Very reasonable and accurate results have been derived.

As the numerical application, the present study was applied to test of flood inundation occurred by dam-break. The results of dam-break flow simulation in experimental channel have been plotted in hydrographs at some gauging points. Based on the comparison of numerical results with measurements, it is clear that the numerical model developed in this study can exactly calculate the flood propagations.

ACKNOWLEDGMENTS

The financial support of the Korea Research Foundation (KRF-2007-313-D00827) is gratefully acknowledged

REFERENCES

Bermudez, A. and Va´zquez, M.E. (1994), Upwind methods for hyperbolic conservation laws with source terms, *Comput. Fluids,* 23, pp.1049-1071.

Billett, S.J. and Toro, E.F. (1997), On WAF-type schemes for multidimensional hyperbolic conservation laws, *Journal of Computational Physics archive,* 130(1), pp.1-24.

Fraccarolo, L. and Toro, E.F. (1995), Experimental and numerical assessment of the shallow water model for two-dimensional dam-break type problems, *Journal of Hydraulic Research*, 33, pp.843-864.

Frazão, S., Sillen, X. and Zech, Y. (1998), Dam-break Flow through Sharp Bends Physical Model and 2D Boltzmann Model Validation, Proceedings of the CADAM meeting, Wallingford, UK.

Gallouët, T., Herard, J.M. and Seguin, N. (2003), Some approximate Godunov schemes to compute shallow-water equations with topography, *computers and Fluids*, 32, pp.478-513.

Goutal, N. (1997), He-43/97/016B, Proceedings of the 2nd workshop on dam-break wave simulaion: Department Laboratoire National d'Hydraulic, Groupe Hydraulic Fluviable Electricite de Fracne, France.

Harten, A., Lax, P.D., and van Leer, B. (1983), On upstream differencing and Godunov-type schemes for hyperbolic conservation law, *Society for Industrial and Applied Mathematics,* 25, pp.35-61.

Hubbard, M.E. and Garcia-Navarro, P. (2000), Flux difference splitting and the balancing of source terms and flux gradients, *J. Comput. Phys,* 165, pp.89-125.

Ingram, D.M., Causon, D.M. amd Mingham, C.G. (2003), Developments in Cartesian cut cell methods, *Mathematics and Computers in Simulation*, 61, pp.561-572.

LeVeque, R.J. (1998), Balancing source terms and flux gradients in high-resolution Godunov methods: The quasi-steady wavepropagation algorithm, *J. Comput. Phys,* 146, pp. 346-365.

Morris, M. (2000), CADAM: Concerted action on dambreak modeling, *Final report*.

Toro, E.F. (1999), *Riemann solvers and numerical methods for fluid dynamics*, Springer, New York.

Văsquez-Cendón, M.E. (1999), Improved treatment of source terms in upwind schemes for the shallow water equations in channels with irregular geometry, *Journal of Computational Physics*, 148, pp.497-526.

Zhou, J.G., Causon, D.M., Mingham, C.G. and Ingram, D.M. (2001), The surface gradient method for the treatment of source terms in the shallow-water equations, *Journal of Computational Physics*, 168, pp.1-25.